



Full Text View

[Volume 31, Issue 7 \(July 2001\)](#)

Journal of Physical Oceanography

 Article: pp. 1698–1711 | [Abstract](#) | [PDF \(232K\)](#)

Upward Momentum Transfer in the Marine Boundary Layer

A. A. Grachev*

Cooperative Institute for Research in Environmental Sciences, University of Colorado, and NOAA/Environmental Technology Laboratory, Boulder, Colorado

C. W. Fairall

NOAA/Environmental Technology Laboratory, Boulder, Colorado

(Manuscript received May 17, 2000, in final form September 6, 2000)

DOI: 10.1175/1520-0485(2001)031<1698:UMTITM>2.0.CO;2

ABSTRACT

This paper focuses on the study of momentum flux between ocean and atmosphere in light winds and is based on the data collected during several field campaigns, the Atlantic Stratocumulus Transition Experiment, the Tropical Ocean Global Atmosphere Coupled Ocean–Atmosphere Response Experiment, and the San Clemente Ocean Probing Experiment. Weak wind at sea is frequently accompanied by the presence of fast-traveling ocean swell, which dramatically affects momentum transfer. It is found that the mean momentum flux (uw covariance) decreases monotonically with decreasing wind speed, and reaches zero around a wind speed $U \approx 1.5\text{--}2 \text{ m s}^{-1}$, which corresponds to wave age $c_p/U \approx 10$ for wave/swell conditions of the experiments in this study. Further decrease of the wind speed (i.e., increase of the wave age) leads to a sign reversal of the momentum flux, implying negative drag coefficient. Upward momentum transfer is associated with fast-traveling swell running in the same direction as the wind, and this regime can be treated as swell regime or mature sea state. In the swell regime the surface stress vector is nearly opposite to wind and swell directions, and the wind is roughly aligned in the swell direction. Thus, a weak wind over ocean swell can be frequently associated with upward momentum transfer (i.e., from ocean to atmosphere).

1. Introduction

Determination of momentum, heat, and mass exchange over the sea is a challenging problem in the modeling of the

Table of Contents:

- [Introduction](#)
- [Wave-induced momentum](#)
- [Field data analysis](#)
- [Summary and discussion](#)
- [REFERENCES](#)
- [TABLES](#)
- [FIGURES](#)

Options:

- [Create Reference](#)
- [Email this Article](#)
- [Add to MyArchive](#)
- [Search AMS Glossary](#)

Search CrossRef for:

- [Articles Citing This Article](#)

Search Google Scholar for:

- [A. A. Grachev](#)
- [C. W. Fairall](#)

coupled atmosphere–ocean system. Understanding of the air–sea fluxes are of obvious relevance for climate modeling, weather forecasting, environmental impact studies and other important applications.

The momentum flux, τ , (or wind stress) is a key parameter in many air–sea interaction studies. First, turbulence over the sea surface is usually associated with mechanical turbulence; second, wind generates the capillarity and gravity sea-surface waves, develops the ocean mixed layer, and is a driving force for ocean local currents. A detailed understanding of the relationship between wind stress and sea state is of renewed importance in the application of various surface scattering radar techniques since it is not the wind itself but the wind-driven waves that determine the microwave signature of the surface.

One major difference between airflow over the sea as contrasted with over land is that the sea surface is mobile. This leads to a limitation in the use of classical theory to describe the marine surface layer, as the surface waves modulate velocity and pressure perturbations emanating upward from the surface. Therefore, the structure of the stress and velocity profiles over sea waves may deviate from similar overland situations. This wave-induced motion gives an additional Reynolds stress to the turbulent and the viscous stresses. The amplitude of wave-induced pressure perturbations falls off exponentially with height ([Elliott 1972](#); [Hsu et al. 1981](#); [Chalikov and Belevich 1993](#); [Hare et al. 1997](#)). It is generally believed that the layer where the wave-induced influence cannot be neglected [the wave boundary layer (WBL)] is typically only one to two wave heights [$O(1\text{ m})$], that is, a small fraction of a wavelength. However, the WBL may extend considerably higher for light winds (see further discussion below).

The influence of surface waves on the turbulent structure of the surface layer has been reported in a number of field studies (e.g., [Volkov 1968, 1969, 1970](#); [Kitaigorodskii 1970](#); [Davidson 1970, 1974](#); [Davidson and Frank 1973](#); [Benilov et al. 1974](#); [Makova 1975, 1977](#); [Antonia and Chambers 1980](#); [Huang et al. 1986](#)) and laboratory experiments (e.g., [Harris 1966](#); [Lai and Shemdin 1971](#); [Takeuchi et al. 1977](#); [Hsu et al. 1981](#); [Anisimova et al. 1982](#)). It has been established that wave-induced perturbations cause distinct peaks in the power spectral densities of the longitudinal, or streamwise, u , and especially of the vertical, w , wind velocity components. Distinct peaks in the power spectra of w and u have been observed to occur at or near the frequency of the maximum in the surface wave spectrum. Theoretical formulations for wind–wave coupling have ranged from the initial quasi-laminar models ([Miles 1957](#)) and turbulence closure models (e.g., [Yefimov 1970](#); [Davis 1972](#); [Li 1995](#)) to current wind–wave coupled models (e.g., [Janssen 1989, 1991](#); [Nordeng 1991](#); [Caudal 1993](#); [Makin et al. 1995](#)). Most recently, direct numerical simulation (DNS) has been applied to turbulent flow over idealized fixed and moving waves (e.g., [Sullivan et al. 2000](#)). Other relevant references on theoretical and numerical modeling can be found in [Belcher and Hunt \(1998\)](#) and [Sullivan et al. \(2000\)](#).

Some information on the dependence of stress on sea state is contained in the wave spectrum. In many past field programs, wave spectral data are lacking and the sea state is described in terms of wave age c_p/u_* , or $c_p/U \cos\theta$, where c_p is the phase speed of the component in the peak of the spectrum, u_* is the friction velocity, U is the mean wind speed, and θ is the relative angle between the wind and wave directions. Representing the waves by wave age implies that most of the wave energy is contained in a narrow range around the peak frequency in the wave spectrum (dominant waves). According to the wave age, the sea state is classified into young (or developing) sea, $c_p/U \cos\theta < 1.2$ and mature sea, $c_p/U \cos\theta > 1.2$ ([Pierson and Moskowitz 1964](#); [Donelan 1990](#)).

Young, short gravity waves that travel much more slowly than the wind extract momentum from the wind, and that energy is conveyed to the surface waves. Actively growing waves transfer energy to longer, faster traveling waves with phase speeds that approach or even slightly exceed the wind speed. With increasing duration and fetch, waves reach equilibrium and are then said to be “saturated.”

A completely different type of situation occurs with a mature sea (swell regime). Eddy-correlation flux observations by [Volkov \(1968, 1970\)](#) and [Kitaigorodskii \(1970\)](#) on the Mediterranean Sea and by [Davidson \(1970\)](#) on Lake Michigan indicate an upward transport of momentum (i.e., from water to air) in the case of a very old sea when the wind speed is much less than the phase speed of the wave spectral peak. Previously, [Harris \(1966\)](#) found in indoor wave tank experiments that progressive waves in water produce an airflow with a mean component in the direction of wave propagation (wave-driven wind). In succeeding years a number of field observations ([Anisimova and Speranskaya 1970](#); [Davidson and Frank 1973](#); [Makova 1975, 1977](#); [Chambers and Antonia 1981](#); [Smedman et al. 1994](#)) and laboratory studies ([Anisimova et al. 1982](#)) provided further evidence of the upward momentum transfer and wave-driven wind ([Anisimova et al. 1978](#)). However, these studies have been limited in scope.

Recently, [Wetzel \(1996\)](#), [Drennan et al. \(1999\)](#), and [Smedman et al. \(1999\)](#) have reexamined the topic of air–sea interaction in the swell regime. These papers discuss different aspects of the problem. The work of [Wetzel \(1996\)](#) based on data obtained from R/P *FLIP* during the Marine Boundary Layer (MBL) Experiment in spring 1995 focuses mostly on the vertical structure of the wave-induced momentum flux; the study is limited to wave age $c_p/U \leq 3.4$, when τ is still positive. [Drennan et al. \(1999\)](#) reported only a few cases of upward momentum transfer measured in Lake Ontario. [Smedman et al. \(1999\)](#) essentially describe a near-neutrally stratified marine boundary layer in a swell regime with very small positive momentum flux at the surface, that is, $\tau \approx 0$, and examine, among other issues, the effect of surface waves on vertical wind

profiles.

It should be noted that the situation in which momentum is transported from ocean to atmosphere, implying negative drag coefficient, is usually associated with decaying wind conditions, for example, after the passage of a storm or gale (e.g., [Kitaigorodskii 1970](#); [Smedman et al. 1994](#)). During such situations, the wind speed drops from about 15–20 m s⁻¹ to about 2–5 m s⁻¹, but waves still travel with high phase velocities. Note that upward momentum transfer up to now has been considered an exotic case.

In this paper, based on the data collected during several field campaigns and literature review, it will be shown that light winds over the open ocean can usually be associated with mature sea states, and often with upward momentum transfer. Locally calm weather at sea is often characterized by the presence of ocean swell, which travels faster than the local wind. Swell produced by a storm can travel for thousands of kilometers across the ocean, carrying considerable energy. Swell propagating into a light wind observation region has a period and wavelength that is not associated with the local wind field. One might expect that arriving swell will affect the local wind field and will drive wind in the direction of swell propagation, that is, induce a wave-driven wind (cf. [Harris 1966](#)). Commonly, swell generated by storms in high latitudes and/or trade wind regions, in both Northern and the Southern Hemispheres, often reaches the Tropics and the equatorial regions where weather is usually calm. However, the light wind regime is rarely considered in the literature in this context, perhaps because of lack of reliable data. Identification of the light-wind-speed regime as a mature sea state (the swell regime) can radically alter our point of view on momentum transfer in light winds. According to [Grachev et al. \(1997\)](#), the light-wind-speed regime (less than 2 m s⁻¹) occurs about 16% of the time in the equatorial west Pacific Ocean (TOGA COARE site). Therefore, reverse momentum transfer is not necessarily an exotic condition. It means that the sea absorbs momentum and kinetic energy in one location and returns a portion back to the atmosphere at a different location. One might expect that the effect could have an impact on climate variability in equatorial regions since the warm pool area in the Pacific Ocean is usually associated with weak winds (e.g., [Fairall et al. 1996a](#)). Thus, it seems likely that, in contrast to sensible and latent heat fluxes in light winds (e.g., [Fairall et al. 1996a](#); [Godfrey and Beljaars 1991](#)), the momentum transfer through the sea surface in this regime could be partially controlled by the sea state as well as shear-stress and stability effects.

In this paper we examine momentum flux transfer at sea in a light-wind-speed regime, which is usually accompanied by the presence of swell. This study is based on an analysis of direct measurements of turbulent air–sea fluxes and surface wave parameters collected by the National Oceanic and Atmospheric Administration Environmental Technology Laboratory (ETL) during several sea campaigns in recent years. Our work deals with “older” sea states than in most previous studies (e.g., [Wetzel 1996](#); [Drennan et al. 1999](#)) because we consider light winds. Secondly, we focus on swell conditions in the open ocean. [Drennan et al.'s \(1999\)](#) measurements were carried out in Lake Ontario, and the measurements of [Smedman et al. \(1994, 1999\)](#) were taken from a small island in the Baltic Sea near Sweden.

We begin with a discussion of various concepts in wave-induced momentum transfer ([section 2](#)), briefly describe the experimental measurements ([section 3a](#)), and then present the results of our analysis of wind and wave fields in surface stress ([section 3b](#)). The results are discussed in [section 4](#).

2. Wave-induced momentum flux

Over ocean waves, the total velocity can be separated into three parts: the mean, turbulent, and wave-induced components of the flow (e.g., [Hare et al. 1997](#)). This results in the decomposition of the total stress at the sea surface, $\boldsymbol{\tau}$, into three constituents: turbulent shear stress, $\boldsymbol{\tau}_{\text{turb}}$, wave-induced stress, $\boldsymbol{\tau}_{\text{wave}}$, and viscous stress, $\boldsymbol{\tau}_{\text{visc}}$, ([Phillips 1977](#)):

$$\boldsymbol{\tau}(z) = \boldsymbol{\tau}_{\text{turb}}(z) + \boldsymbol{\tau}_{\text{wave}}(z) + \boldsymbol{\tau}_{\text{visc}}(z), \quad (1)$$

where

$$\begin{aligned} \boldsymbol{\tau} &= -\rho_a(\langle uw \rangle \mathbf{i} + \langle vw \rangle \mathbf{j}), \\ \boldsymbol{\tau}_{\text{turb}} &= -\rho_a(\langle u'w' \rangle \mathbf{i} + \langle v'w' \rangle \mathbf{j}), \\ \boldsymbol{\tau}_{\text{wave}} &= -\rho_a(\langle \tilde{u}\tilde{w} \rangle \mathbf{i} + \langle \tilde{v}\tilde{w} \rangle \mathbf{j}). \end{aligned} \quad (2)$$

Here ρ_a is air density, angle brackets are time and/or spatial averaging operators, primes denote turbulent fluctuations, the $\tilde{}$ denotes wave-induced fluctuations, (u, v, w) are the longitudinal (x axis), lateral (y axis), and vertical (z axis) components, respectively, and \mathbf{i} and \mathbf{j} represent the longitudinal and lateral unit vectors. In the general case (x, y, z) is the fixed reference frame, although it is common practice to align the x axis with wind direction. For simplicity, the viscous stress in [\(2\)](#) is omitted. In the spectral form we can express the stress components as

$$\begin{aligned}
\langle uw \rangle &= \int_0^{+\infty} C_{uw}(f) df, \\
\langle u'w' \rangle &= \int_0^{+\infty} C_{u'w'}(f) df, \\
\langle \tilde{u}\tilde{w} \rangle &= \int_0^{+\infty} C_{\tilde{u}\tilde{w}}(f) df, \quad (3)
\end{aligned}$$

where $C_{uw}(f)$, $C_{u'w'}(f)$, and $C_{\tilde{u}\tilde{w}}(f)$ are the uw cospectra of the total, turbulent, and wave-induced stress constituents, respectively (f is the frequency in Hz). The corresponding $\mathfrak{U}w$ cospectra are derived in a similar manner by the simple replacement of the u symbol in (3) with a \mathfrak{U} symbol. It is important to keep in mind that measurement of the *total* stress, τ (i.e., $\langle uw \rangle$ and $\langle \mathfrak{U}w \rangle$), is a straightforward application for a sonic anemometer.

The stress at the surface is the tangential force per unit area exerted by the wind on the surface. It results in a transfer of horizontal momentum between the air and sea via vertical momentum flux. Thus, the stress is a horizontal vector (τ), whereas the momentum flux (τ) can be viewed as directed upward or downward. If the stress at the sea surface is facing in the wind direction, the momentum flux is directed downward ($\tau > 0$) and vice versa ($\tau < 0$). Stress magnitude is numerically equal to the momentum flux, that is, $|\tau| = \tau$, $|\tau_{\text{turb}}| = \tau_{\text{turb}}$ and $|\tau_{\text{wave}}| = \tau_{\text{wave}}$. Therefore, it is common practice to not differentiate between stress and momentum flux.

The wave-induced momentum flux, $\tau_{\text{wave}}(z)$ (the form drag, or pressure drag), is described by the pressure–wave slope correlation at the surface (Hare et al. 1997). It is assumed (e.g., Janssen 1989, 1991; Nordeng 1991; Caudal 1993; Makin et al. 1995) that $\tau_{\text{wave}}(z)$ at the wave surface $z = \eta$ may be described by the wave spectrum $S(\omega)$:

$$\tau_{\text{wave}}(\eta) = \rho_w \int_0^{+\infty} \beta_w g \omega c_p^{-1} S(\omega) d\omega, \quad (4)$$

where ρ_w is water density, g is the acceleration due to gravity, $\omega = 2\pi f$, and β_w is the dimensionless wind–wave interaction parameter (or the wave growth parameter).

The wave-induced momentum flux in the marine surface layer shows strong dependence on wave age (e.g., Makova 1975, 1977; Sullivan et al. 2000). For young or developing seas $\theta \approx 0$ and the wave-induced momentum flux is downward; that is, $\tau_{\text{wave}} > 0$. However, τ_{wave} decreases for increasing wave age, reaches zero, and reverses sign; $\tau_{\text{wave}} < 0$. Unlike τ_{wave} , the turbulent momentum flux is always positive; that is, $\tau_{\text{turb}} > 0$. Further increase of the wave age tends to enhance the negative portion of the total momentum flux and finally leads to a sign reversal of τ (i.e., $\tau = \tau_{\text{turb}} + \tau_{\text{wave}} < 0$), indicating a transfer of momentum from the ocean to the atmosphere. The drag coefficient under these conditions is negative, and the practice of transforming meteorological data to equivalent neutral conditions is not valid (see Drennan et al. 1999).

Based on a spectral analysis of field data, Makova (1975, 1977) identified three different regimes of wind–wave interaction. She found that the wave-induced momentum at the surface is transported from ocean to atmosphere when $U/c_p < 0.6$ (or $c_p/u_* > 50$), although only two cases ($U = 2.1$ and 2.4 m s^{-1} , and $U/c_p = 0.13$ and 0.15 , respectively) of upward momentum transfer observed in the Atlantic were reported. According to three different turbulent closure calculations by Li (1995), $\tau_{\text{wave}}(\eta)$ reverses sign at $c_p/u_* = 23\text{--}28$ [or $c_p/U \approx 0.8$; see, e.g., Fig. 10 in Sullivan et al. (2000)]. Based on DNS Sullivan et al. (2000) find that at $c_p/u_* > 14$ (or $c_p/U > 0.6$) the wave-induced momentum changes sign and acts to drive wind. Classifications by Belcher and Hunt (1998) predict fast waves for $c_p/u_* > 25$. Despite the different values of c_p/u_* for the point when $\tau_{\text{wave}}(\eta)$ reverses sign obtained in these studies, the transition value based on c_p/U is close to unity in each.

Smedman et al. (1994, 1999) describe the cases of a near–neutrally stratified marine surface layer with no shear

production near the surface, that is, $\tau = \tau_{\text{turb}} + \tau_{\text{wave}} \approx 0$ since $\tau_{\text{turb}} > 0$ and $\tau_{\text{wave}} < 0$. Wave-induced perturbations were

observed in a layer extending to at least 26 m, and the 10-m drag coefficient was about 0.7×10^{-3} for $c_p/U \approx 1.2$.

However, in spite of very low total momentum flux, the turbulence intensity was high. According to [Smedman et al. \(1994, 1999\)](#) this was caused by so-called inactive turbulence, which is imported by pressure transport from layers in the upper parts of the atmospheric boundary layer (ABL).

It is notable that negative covariance momentum flux in light winds over the open ocean has been reported by [Fairall et al. \(1996a\)](#) for TOGA COARE data obtained from two different platforms: R/V *Moana Wave* ([Fairall et al. 1996a](#), their Fig. 10b) and from the National Center for Atmospheric Research Electra aircraft ([Fairall et al. 1996a](#), their Fig. 12c). Recently [Edson et al. \(1998\)](#) reported upward momentum flux events during the MBL Experiment. Positive values of $\langle uw \rangle$ have been obtained at the same time from R/V *Wecoma* and R/P *FLIP* when the ship was within 50 km of *FLIP* ([Edson et al. 1998](#), Figs. 17–19, 21). However, these cases were treated as sampling uncertainties. The measurements made from the low-altitude Electra aircraft during TOGA COARE and data by [Smedman et al. \(1994\)](#) both indicate that the upward momentum flux can occupy the entire ABL. Based on simultaneous airborne and mast measurements, [Smedman et al. \(1994\)](#) observed that momentum flux directed from the sea to the atmosphere occupied the lowest 200 m of the ABL [Fig. 3b in [Smedman et al. \(1994\)](#)]. Thus, the assumption that a 10-m measurement level is beyond the WBL may not be true for light winds. It is worth noting that simultaneous measurements from the separate platforms by [Edson et al. \(1998\)](#) show that the upward momentum flux can exist over sufficiently large areas of the open ocean.

The inertial dissipation method (which a priori leads to positive values of τ) is extensively used for determination of the momentum flux from turbulent measurements on ships. It is likely that this is a reason why the concept of the upward momentum transfer at weak winds is not widely accepted until now. For example, [Dobson et al. \(1994\)](#) investigated the stress in the swell regime, but they used the inertial dissipation technique. Obviously, we must now reconsider applicability of the inertial dissipation method to compute τ in a swell regime (see also [Drennan et al. 1999](#)).

It is likely that fluxes derived from analyses of the high-frequency portion of the inertial subrange can be applied to determine the τ_{turb} in [Eq. \(1\)](#). This portion of the spectrum may be free from wave-induced perturbations since significant peaks in the turbulence spectra occur at lower frequencies near dominant wave peaks typically of order 0.1–1 Hz (e.g., [Kitaigorodskii 1970](#)). Recently, [Edson et al. \(1997\)](#) showed that the dimensionless dissipation function depended on wave age. Thus, the issue of whether or not τ_{turb} can be derived from the high-frequency portion of velocity spectra using the Monin–Obukhov similarity-based inertial dissipation technique (e.g., [Fairall and Larsen 1986](#)) remains open.

Laboratory experiments by [Anisimova et al. \(1982\)](#) and field observations by [Anisimova and Speranskaya \(1970\)](#), [Davidson and Frank \(1973\)](#), and [Smedman et al. \(1994\)](#) showed examples where the *total* momentum flux τ was negative near the sea surface but reversed sign higher up. However, current wind–wave models assume stationarity and homogeneity, which implies that the total stress [\(1\)](#) is constant with height. Furthermore, some formulations (e.g., [Nordeng 1991](#)) allow only positive values for β_w ; this causes $\tau_{\text{wave}}(z) > 0$ [i.e., waves only extract momentum from air; see [\(4\)](#)]. A model capable of reproducing the upward momentum transfer requires a parameterization of τ_{wave} , which is negative for wave components with $c_p/U \geq 1$, that is, for long waves (swell) traveling faster than wind.

A clear physical basis underlies the upward momentum transfer. When two particles (e.g., water and air) traveling in the same direction with different velocities contact one another, the faster particle will accelerate the other particle that moves more slowly. Therefore, the momentum flux will be directed from a fast particle to a slow particle. The mechanism that transports momentum between particles may be viscous forces (as in the above example) or pressure fluctuation induced by the waves (swell) traveling faster than the wind.

Laboratory studies (e.g., [Harris 1966](#); [Lai and Shemdin 1971](#); [Anisimova et al. 1982](#)) conducted over mechanically generated monochromatic waves represent idealized situations where wave energy is concentrated within a narrow frequency range around a well-defined peak in the surface-wave spectrum. In contrast, wave-induced disturbances over natural oceanic waves tend to occur over a broad frequency band. The sea surface is usually treated as a superposition of waves traveling with different velocities (e.g., [Makin et al. 1995](#)). Thus, a portion of spectral components of surface waves produces downward momentum and another part is associated with upward momentum flux, that is, from waves to air. Short gravity waves that travel with slower phase speed relative to the wind are sinks of momentum; that is, they extract momentum from air, whereas long waves (swells) traveling faster than the wind and running in the same direction as the wind are sources of momentum, that is, they produce upward momentum flux. However, it is not clear that the pressure-induced growth of short waves is unaffected by the presence of swell.

3. Field data analysis

In this section we use data collected by the NOAA/ETL Air–Sea Interaction Group on five cruises during three field

programs to examine the behavior of momentum transfer in light winds. Data were taken on board the R/V *Malcolm Baldrige* in June 1992 during the Atlantic Stratocumulus Experiment (ASTEX), on board the R/V *Moana Wave* in 1992–93 (three separate cruises) during TOGA COARE, and from the R/P *FLIP* in September 1993 during the San Clemente Ocean Probing Experiment (SCOPE).

a. Measurements and instrumentation

Some details about ASTEX are given by [White et al. \(1995\)](#) and [Fairall et al. \(1997\)](#). The TOGA COARE and SCOPE data are described in [Fairall et al. \(1996a–c\)](#), [Grachev and Fairall \(1997\)](#), and [Grachev et al. \(1997, 1998\)](#). Thus, only a brief sketch will be given here. An identical seagoing flux system was used in these experiments, and a detailed description of the measuring system can be found in [Fairall et al. \(1997\)](#). Platform motion corrections were made as described by [Edson et al. \(1998\)](#). A sonic anemometer/thermometer and a high-speed infrared hygrometer were used to make the measurements of turbulent fluxes. Data include 50-min-averaged observations of covariance and inertial dissipation estimates of the turbulent fluxes of momentum, sensible and latent heat, mean meteorological variables, radiation fluxes, and the convective boundary layer height. Direct measurements of the sea-surface wave parameters were made only in SCOPE. Several data quality indicators have been applied to the original atmospheric datasets. Data have been edited for unfavorable relative wind directions, mean wind vector tilt, a maneuver of the ship during the record, contamination of the turbulence data by the ship's wake, precipitation, and salt contamination. Based on established criteria, the best flux estimate from the data has been used. For example, all ASTEX measurements in wind speed range 0–1 m s⁻¹ have been rejected.

The ASTEX cruise on the R/V *Malcolm Baldrige* took place in the eastern Atlantic Ocean, between 27° and 37°N, 22° and 27°W as part of a program focused on measurements of the dynamics and microphysical optical properties of marine clouds. The turbulence and bulk meteorological measurements in ASTEX were made 21 m above the sea surface. The same instruments were at 15 m for TOGA COARE and 11 m for SCOPE. In TOGA COARE, measurements were carried out from the R/V *Moana Wave* for three cruise legs in the tropical warm pool area, western Pacific Ocean. The ship usually operated in a “drift” mode for ocean microstructure measurements.

In the SCOPE experiment the R/P *FLIP* was moored about 15 km northwest off the northwest point of San Clemente Island (off the southern California coast) with good open ocean exposure for northwest winds. Surface wave parameters were measured by the Air–Sea Interaction Array designed and constructed for SCOPE. This system included underwater pressure sensors to measure gravity waves, as well as a capacitance wire capillary wave array that responded to frequencies up to 25 Hz. These sensors were mounted on a mast deployed from one of the horizontal booms on *FLIP*. The underwater pressure sensors, located about 1.7 m underwater, were in a square array, on 2.1-m aluminum struts. The atmospheric pressure sensors were located directly above the underwater pressure sensors, 2 m above the mean ocean surface. The capillary wave array consisted of four capacitance wires in a square array, 1 cm on a side. This array was mounted on a buoy so that it would “wave ride.” The wave-riding arm was oriented in the direction from which most wave activity was expected without being downstream of *FLIP* (i.e., the northwest).

b. Results

[Figures 1a–c](#) show the averaged downstream stress component (eddy correlation), $\tau_x = -\rho_a \langle uw \rangle$, plotted against mean wind speed for the ASTEX (a), TOGA COARE (b), and SCOPE (c) data, respectively. Hereinafter the x axis is aligned with the mean wind. In [Fig. 1](#) we present data only for the light and moderate wind speeds ($U \leq 6$ m s⁻¹). A positive sign of τ_x corresponds to downward momentum transfer (i.e., from atmosphere to ocean) and vice versa. The results from [Fig. 1](#) indicate that the τ_x measured at fixed height decreases monotonically for decreasing wind speed, and it reaches zero at a wind speed of about 1.5–2 m s⁻¹. Further decrease in wind speed leads to a sign reversal of the momentum flux, implying negative drag coefficient. Thus, the momentum flux reaches zero and reverses sign before U reaches zero, differing from the traditional point of view which assumed that τ_x and U reach zero hand-in-hand. The slightly greater scatter for the ASTEX ([Fig. 1a](#)) and TOGA COARE ([Fig. 1b](#)) data as compared with the SCOPE data ([Fig. 1c](#)) is the result of more variable meteorological conditions and the use of a conventional ship, which is a less-ideal observing platform than *FLIP*. However, all data in [Figs. 1a–c](#) verify upward momentum transfer in light winds. Note that the transition wind speed value, $U \approx 1.5$ –2 m s⁻¹ is approximately the same for all datasets considered here.

As mentioned above, the momentum transfer in light winds (swell regime) is basically controlled by the sea state. Therefore, τ_x should be described in terms of wave age, for example, $c_p/U \cos\theta$, rather than wind speed, as in [Fig. 1](#). We use U in [Fig. 1](#) because air–sea fluxes measured onboard a conventional ship (e.g., during ASTEX and TOGA COARE) usually are not accompanied by special measurements of sea wave parameters and because swell in the open ocean tends to have nearly fixed frequency (and, therefore, c_p). Typical open ocean swell periods are $T \approx 10$ –25 s, corresponding to wave lengths $L = (g/2\pi)T^2 \approx 150$ –1000 m ([Kinsman 1965](#)). Note that moored (e.g., R/P *FLIP*) or fixed platforms are

more suited to wave measurements. In order to enhance the interpretation of Fig. 1 (a), we include a simple analysis of the stress direction based on the routine visual observation of the swell made by observers from the ship bridge. Momentum flux presented in Figs. 1a–c has been sorted into two groups according to the relative wind–swell directions (Table 1). Since we are interested in events of upward momentum transfer, only light winds, up to 2 m s^{-1} , are presented in Table 1. According to data in Table 1 the averaged momentum flux associated with swell running in the same direction with wind is less (or negative) than the momentum flux associated with counterswell runs. This statement is also supported by the data reported in Donelan et al. (1997) and Drennan et al. (1999, Fig. 10). Thus, upward momentum transfer, $\tau_x < 0$, is generally characterized by conditions when swell is running in the same direction as the wind. However some individual 50-min flux samples $\tau_x < 0$ in Fig. 1 and Table 1 associated with counterswell runs may reflect the sampling scatter. Among other things, the bridge wave observations were made on an hourly basis during ASTEX and only once every 4 hours during TOGA COARE.

Because air–sea fluxes in SCOPE were measured coincidentally with sea surface variables, we consider the SCOPE data in more detail. The entire SCOPE time series for several key variables are summarized in Figs. 2 and 3 (see also Fairall et al. 1996c). The marine surface layer was, with the exception of a few days of fog, unstable for the duration of SCOPE; winds were not strong, averaging around 4 m s^{-1} . The northwest swell was moderate but almost always present, and the direction of the waves was very constant (about 300°). The maximum value of the wind velocity was about 11 m s^{-1} on one brief occasion. During several runs the environmental conditions were characterized by mostly unstable stratification when wind velocities were below 1 m s^{-1} . Wind directions were predominantly from the northwest, but the influence of the mesoscale land–sea contrast caused some modulation on a diurnal cycle. Several episodes of weakening and turning winds occurred in which the wind direction and sea direction were out of balance. These episodes caused a loss of streamwise (uw) covariance and tended to cause nonzero crosswind ($\mathcal{U}w$) covariance (see Fig. 3). Notice that in this paper all directions for wind, waves, and stress are calculated using the meteorological conventions (“from”).

Figure 4 presents individual observations (50-min averaged) of the uw -component momentum flux (eddy correlation) versus mean wind speed (a) and inverse wave age, $U \cos\theta/c_p$, (b) for the SCOPE data. Figure 4b contains less data than Fig. 4a because not all turbulent data were accompanied by surface wave measurements (see Fig. 3). Figure 4b shows that the momentum flux changes sign in the range of $U \cos\theta/c_p$ from about 0.05 to 0.2 where the wind speed is generally between 1 and 3 m s^{-1} (Fig. 4). The midrange of values where the stress reverses the sign is 0.1 for the inverse wave age (i.e., wave age is 10) and 2 m s^{-1} for wind speed. The data in Fig. 4 marked by solid triangles represent cases when the wind speed vector has a component opposite to wave propagation, that is, $U \cos\theta/c_p < 0$. In these light-wind and counterswell runs the momentum is generally transported downward from the atmosphere to the sea (cf. appropriate points in Figs. 4a and 4b). This result is consistent with the ASTEX and TOGA COARE data (Table 1) and the enhancement of the stress for the counterswell runs reported by Donelan et al. (1997) and Drennan et al. (1999).

It should be emphasized that the above obtained transition values $U \approx 2 \text{ m s}^{-1}$ and $c_p/U \cos\theta \approx 10$ are not universal constants. For instance, the Drennan et al. (1999) datasets include a number of upward momentum flux runs at U around 4 m s^{-1} ($c_p/U \approx 2$). According to Eq. (1) the total momentum flux, τ , is the sum of τ_{turb} and τ_{wave} and behavior of τ depends on the mutual contribution of both components (for simplicity only colinear wind and swell case is considered here). The turbulent momentum flux is always positive, $\tau_{\text{turb}} > 0$, while the wave-induced momentum flux, τ_{wave} , may be positive or negative. One would expect that the magnitude of τ_{wave} is dependent on the significant wave height, H_S , or wave slope. An increase of wave amplitude should lead to an increase of magnitude of τ_{wave} (negative in the swell regime), and therefore it leads to increasing of the transition wind speed value for τ (decreasing transition wave age value). This conclusion correlates with H_S reported by Drennan et al. (1999, Table II), $H_S = 1.11\text{--}1.45 \text{ m}$, and the SCOPE values $H_S \approx 0.5 \text{ m}$ (see Fig. 3). The wave-induced momentum flux reverses sign supposedly at $c_p/U \approx 1$ (e.g., Makova 1975, 1977; Li 1995; Sullivan et al. 2000), whereas the total momentum flux changes sign at an older wave age because of the positive τ_{turb} , and the transition point is depended on wave slope or H_S . It seems plausible that our data reflect typical open ocean swells, whereas the Drennan et al. (1999) results correspond to the wave climate in an enclosed lake.

Figure 5 presents directional characteristics of the wind and surface stress vector as a function of the wind speed. True wind direction is shown in the upper panel (a), the relative angle between the stress vector and wind vector [$\arctan(\mathcal{U}w/\langle uw \rangle)$] is plotted in the middle panel (b), and the true stress direction is presented in the bottom panel (c). The same quantities as function of the wave age have been analyzed also but they are not shown here. According to Fig. 5, data may be separated into three categories (except counterswell runs):

1. Strong winds (windsea), $U \gtrsim 5-6 \text{ m s}^{-1}$ ($c_p/U \cos\theta \approx 2$). Wind is generally aligned along the dominant wave direction (300°), and the mean stress direction is also generally in line with the wind and dominant waves direction (Figs. 5b,c). This result agrees with many previous studies, such as Geernaert et al. (1993), Rieder et al. (1994), and Drennan et al. (1999).
2. Moderate winds (transition regime), $1.5-2 \approx U \approx 5-6 \text{ m s}^{-1}$ ($2 \approx c_p/U \cos\theta \approx 10$). In this subrange wind direction is approximately between 210° and 330° (Fig. 5a). As wind speed decreases, the stress vector deviates significantly from wind (Fig. 5b) and swell (Fig. 5c) direction. The stress vector turns through about 180° and finally is nearly opposite to wind and swell direction (Figs. 5b,c). Note that the constant swell direction (300°) is a substantial factor responsible for the behavior of the true stress angle in Fig. 5c.
3. Light winds (swell regime), $U \lesssim 1.5-2 \text{ m s}^{-1}$ ($10 \approx c_p/U \cos\theta$). It turns out that the wind is again aligned with the swell direction in this case (Fig. 5a). The stress vector, on the average, is nearly opposite to wind and swell direction. The regime where the surface stress is aligned opposite to the wind direction corresponds to upward momentum transfer (negative points in Fig. 4). Whereas stress dramatically reverses its orientation (Figs. 5b,c), the wind tends to be colinear with the swell. It may be that the swell drives the wind in the direction of the swell propagation, that is, induces “wave-driven wind” (cf. Harris 1966). Unfortunately, only a limited number of observations in this regime were obtained during SCOPE.

Note that the above classifications are based on the SCOPE data, and in the general case they should be dependent on the significant wave height, H_s , or wave slope (see discussion above).

We now briefly consider the behavior of the stress vector within the WBL in the subrange $U \approx 5-6 \text{ m s}^{-1}$. According to Fig. 5c, the stress vector rotates in a counterclockwise direction as wind speed decreases, that is, from northwest and west through south to approximately east direction. Such rotation is consistent with distribution of the wind angles in Fig. 5a. Namely, wind direction in Fig. 5a deviates from the swell direction (300°), generally to the west and southwest. According to (1) the total surface stress is a vector sum of the turbulent stress and the wave-induced stress, and therefore τ lies between the wind direction and the wave direction, if $\tau_{\text{wave}} > 0$, that is, τ is facing in the wave direction (cf. Geernaert et al. 1993, Rieder et al. 1994). In the case $\tau_{\text{wave}} < 0$ (e.g., light winds and background swell) the total surface stress lies between the wind direction and the opposite wave direction. For better visualization, we consider two cases, $U = 6 \text{ m s}^{-1}$ and 3 m s^{-1} , and in the both cases wind blows from west (270°) and swell direction is 300° (Fig. 5a). When $U = 6 \text{ m s}^{-1}$, supposedly $\tau_{\text{wave}} > 0$ and the stress angle is between 270° and 300° (Fig. 5c). In the case $U = 3 \text{ m s}^{-1}$, supposedly $\tau_{\text{wave}} < 0$ and the stress angle is between 270° and 120° (opposite to the swell angle), that is, stress has approximately the south-southwest direction (Fig. 5c).




Since the stress in light winds is crucially affected by the swell it makes sense to plot a stress component in the swell direction, τ_θ , defined by




$$\tau_\theta = \tau_x \cos\theta + \tau_y \sin\theta, \quad (5)$$

where $\tau_x = -\rho_a \langle uw \rangle$ and $\tau_y = -\rho_a \langle vw \rangle$. Figure 6 shows dependence τ_θ upon mean wind speed (a) and inverse wave age (b). Note that Fig. 6b contains less data points than Fig. 6a for the same reason as Fig. 4b. According to Fig. 6 behavior of τ_θ overall resembles τ_x (Fig. 4); for example, τ_θ reversed sign at about the same wind speed and wave age. This is due to the fact that in many cases the wind is aligned along wave propagation (Fig. 5a). The fundamental difference between τ_x and τ_θ is related to counterswell runs; $\tau_x > 0$, whereas $\tau_\theta < 0$. Departures from this, that is, counterswell runs with $\tau_x < 0$ (Fig. 4) and $\tau_\theta > 0$ (Fig. 6) may be associated with the sampling scatter or neglecting other important factors discussed below.

The view outlined above assumes that τ_{wave} is associated with pure unimodal wave field (e.g., swell). It is clear that such a representation is a simplified vision of the situation. This scheme may be appropriate for a high wind speed regime (pure windsea) or light winds (swell regime). However, the approach fails to describe some observations mentioned above in the transition situations ($1.5 \text{ m s}^{-1} \approx U \approx 6 \text{ m s}^{-1}$ for the SCOPE data). Presumably this regime is associated with a complex sea state, that is, mixed swell and windsea. For such situations the wave-induced stress should be split into two parts, $\tau_{\text{wave}} = \tau_{\text{wave1}} + \tau_{\text{wave2}}$, where τ_{wave1} and τ_{wave2} are due to swell and pure wind waves, respectively. It is thought that each

constituent is governed by its own wave age (two peaks in the wave spectra are expected), with $c_{p1}/U \cos\theta_1 > c_{p2}/U \cos\theta_2$ (here subscripts 1 and 2 are associated with swell and wind waves, respectively). Since the swell usually travels faster and short waves more slowly than the wind, in the majority of cases $|\tau_{\text{wave1}}| < 0$ and $|\tau_{\text{wave2}}| > 0$ (relative to wind direction). Furthermore, in the general case vectors τ_{turb} , τ_{wave1} , and τ_{wave2} are not colinear to one another. All these reasons may result in the observed scatter of the surface stress in magnitude and direction. The main motivation of the study is to investigate the swell regime in light winds (upward momentum transfer) and, for this reason, different aspects of stress behavior under mixed sea conditions are not discussed here.




[Figure 7](#)  shows the evolution of the shapes of the mean uw cospectra, [Eq. \(3\)](#), for light winds in the speed range from 0.3 to 6 m s⁻¹ (SCOPE data). Data are averaged in wind speed bins with 1 m s⁻¹ width. Analysis of data presented in [Fig. 7](#)  indicates that cospectral energy decreases monotonically for decreasing wind speed. Cospectra obtained in the wind speed range 2–6 m s⁻¹ lie in the negative range that corresponds to downward momentum transfer. For winds above 6 m s⁻¹, uw cospectra also have “regular” behavior. Cospectra for the wind speed range 1–2 m s⁻¹ have both negative and positive segments, although cospectra for a wind speed range below 1 m s⁻¹ lie solely on the positive side. Thus, the momentum is transported purely from ocean to atmosphere (across the entire cospectrum) in this wind speed range. This behavior is consistent with the data presented in [Fig. 1c](#) .





One can argue that the scatter of points in [Figs. 1 and 4a](#)  indicates that fluxes at weak winds are relatively unreliable. However, data in [Figs. 4b and 6b](#) , and the shapes of the mean uw cospectra in [Fig. 7](#)  clearly indicate that the upward momentum transfer at light winds is well defined.


4. Summary and discussion


In this paper the behavior of the momentum flux over the sea surface in the light-wind-speed regime has been examined. The results are based on the direct measurements of turbulent air–sea fluxes obtained during several sea expeditions: ASTEX, TOGA COARE, and SCOPE (during SCOPE, simple surface wave parameters were also measured).

The main result of this work is that the light-wind-speed regime at sea is frequently characterized by an inverse (upward) momentum flux when momentum is transported from ocean to atmosphere. The above findings occur because, under light winds and strong swell, long ocean waves (swell) traveling faster than local wind and in the same direction cause upward momentum transport, implying a negative drag coefficient. This regime may be treated as swell regime or mature sea state.

It is found that the momentum flux, τ_x decreases monotonically with decreasing wind speed (increasing wave age), reaches zero, and reverses sign before U reaches zero ([Figs. 1, 4, 6](#) ). The traditional point of view assumes that τ_x and U reach zero hand-in-hand. It is shown that τ_x reverses sign at $c_p/U \cos\theta \approx 10$ ([Figs. 4b, 6b](#) ), corresponding to a wind speed of 1.5–2 m s⁻¹ ([Figs. 4a, 6a](#) ). More generally, these transition values may be dependent on the magnitude of swell, or wave slope.

The distinguishing features of the swell regime as it is found based on the SCOPE data are (i) the surface stress vector, τ , is approximately opposite to the wind direction ([Fig. 5b](#) ) that corresponds to upward momentum transfer ([Fig. 4](#) ) and (ii) τ is opposite to the swell direction ([Fig. 5c](#) ). This is intimately associated with the fact that in this regime wind is nearly aligned with the swell direction ([Fig. 5a](#) ). It is believed that the last may be considered as support of the “the wave-driven wind” concept obtained by [Harris \(1966\)](#) in the tank measurements.

It is found that swell dramatically affects the stress vector direction. As wind speed decreases, the stress vector changes its orientation by approximately 180°, that is, opposite to wind and swell direction ([Figs. 5b,c](#) ) , while wind tends to be colinear with the swell.

Upward momentum transfer in the open ocean is not a rare occurrence. Based on the obtained results we suggest that, in some areas of the ocean, upward momentum transfer occurs about 10% of the time. For typical open-ocean swell conditions, the point where τ_x reverses sign corresponds to a wind speed of 1.5–2 m s⁻¹ ([Fig. 1](#) ). According to [Grachev et al. \(1997\)](#), winds less than 2 m s⁻¹ occur about 16% of time in the TOGA COARE region. Upward momentum transfer can extend over large vertical and horizontal scales. Under conditions of light winds and strong swell the WBL depth extends considerably higher than typical measurement heights, 10 m above sea surface (see also [Smedman et al. 1994](#)).

Our results lead to the following conclusions and recommendations.

1. The common practice of using the friction velocity $u_* = (\tau_x/\rho_a)^{1/2}$ as a scaling parameter (e.g., for wave age, c_p/u_*) evidently is invalid for swell conditions since τ_x reaches zero and changes sign. Thus, the standard Monin–Obukhov similarity theory (MOST) presumably is not applicable to describe the momentum transfer in swell conditions. In a similar manner, use of the traditional neutral drag coefficient, C_{Dn} , which is based on MOST, and the roughness length, $z_o = z \exp(-\kappa/C_{Dn}^{1/2})$, should be reconsidered for the swell regime. However, MOST is still valid for young seas above the WBL (see also [Drennan et al. 1999](#); [Smedman et al. 1999](#)).
2. The eddy-correlation method should be used whenever possible to determine momentum flux across the air–sea interface in light-wind speed regimes rather than inertial dissipation method (see also [Drennan et al. 1999](#)). Present formulations of the inertial dissipation method are based on the MOST and a priori lead to positive values of τ_x .
3. Basic sea-surface wave parameters, such as c_p , wave height, and wave propagation direction (separately for swell and wind waves), must be monitored during field measurements in the light-wind-speed regime. They should be included in the list of the governing parameters along with standard MOST parameters.
4. Present wind–wave coupling models and bulk formulae overlook the above effect and, therefore, overestimate wave-induced stress and momentum input to the ocean at light winds. The high quality stress data collected during a number of field campaigns in recent years make it possible to go from the documentation of the above effect to the parameterization of the phenomenon for the next generation of the wind–wave coupled models and bulk algorithms.

Acknowledgments

This work was partially supported by the NOAA Climate and Global Change Program, the Office of Naval Research (ONR) Marine Boundary Layers Program, and the U.S. Department of Energy (DOE) Atmospheric Radiation Measurements (ARM) Program.

AAG is grateful to Arizona State University (MAE/Environmental Fluid Dynamic Program) for support while some of this work was proceeding. He was also supported by Projects INTAS 96-1692 and EU Project Surface Fluxes in Climate System (SFINCS) under EC Contract ENV4-CT97-0573. Anonymous reviewers helped us to give the paper a sharper focus and clarify the issues.

REFERENCES

- Anisimova E. P., and A. A. Speranskaya, 1970: Air flow structure in the immediate vicinity of the disturbed surface of the water. *Izv. Acad. Sci. USSR, Atmos. Oceanic Phys. (Engl. Transl.)*, **6**, 381–382. [Find this article online](#)
- , S. V. Dobroklonsky, B. M. Lesnikov, and A. A. Speranskaya, 1978: Transformation of wind velocity profiles and drift currents along a wind-generated wave profile. *Izv. Acad. Sci. USSR, Atmos. Oceanic Phys. (Engl. Transl.)*, **14**, 320–322, (4). [Find this article online](#)
- , V. I. Makova, E. A. Nikitina, and A. A. Speranskaya, 1982: Momentum-flux spectrum above a developing wind wave. *Izv. Acad. Sci. USSR, Atmos. Oceanic Phys., (Engl. Transl.)*, **18**, 435–439, (5). [Find this article online](#)
- Antonia R. A., and A. J. Chambers, 1980: Wind-wave-induced disturbances in the marine surface layer. *J. Phys. Oceanogr.*, **10**, 611–622. [Find this article online](#)
- Belcher S. E., and J. C. R. Hunt, 1998: Turbulent flow over hills and waves. *Annu. Rev. Fluid. Mech.*, **30**, 507–538. [Find this article online](#)
- Benilov A. Y., O. A. Kuznetsov, and G. N. Panin, 1974: On the analysis of wind wave-induced disturbances in the atmospheric turbulent surface layer. *Bound.-Layer Meteor.*, **6**, 269–285. [Find this article online](#)
- Caudal G., 1993: Self-consistency between wind stress, wave spectrum, and wind-induced wave growth for fully rough air–sea interface. *J. Geophys. Res.*, **98**, 22 743–22 752.
- Chalikov D., and M. Yu. Belevich, 1993: One dimensional theory of the wave-boundary layer. *Bound.-Layer Meteor.*, **63**, 65–96. [Find this article online](#)
- Chambers A. J., and R. A. Antonia, 1981: Wave-induced effect on the Reynolds shear stress and heat flux in the marine surface layer. *J. Phys. Oceanogr.*, **11**, 116–121. [Find this article online](#)

Davidson K. L., 1970: An investigation of the influence of the waves on the adjacent airflow. Ph.D. thesis, University of Michigan, Ann Arbor, MI, 259 pp.

—, 1974: Observational results on the influence of stability and wind–wave coupling on momentum transfer and turbulent fluctuations over ocean waves. *Bound.-Layer Meteor*, **6**, 305–331. [Find this article online](#)

—, and A. J. Frank, 1973: Wave-related fluctuations in the airflow above natural waves. *J. Phys. Oceanogr*, **3**, 102–119. [Find this article online](#)

Davis R. E., 1972: On prediction of the turbulent flow over a wavy boundary. *J. Fluid Mech*, **52**, 287–306. [Find this article online](#)

Dobson E. W., S. D. Smith, and R. J. Anderson, 1994: Measuring the relationship between wind stress and sea state in the open ocean in the presence of swell. *Atmos.–Ocean*, **32**, 237–256. [Find this article online](#)

Donelan M. A., 1990: Air–sea interaction. *The Sea*. Vol. 9: *Ocean Engineering Science*, B. LeMehaute and D. M. Hanes, Eds., John Wiley and Sons, 239–292.

—, W. M. Drennan, and K. B. Katsaros, 1997: The air–sea momentum flux in conditions of wind sea and swell. *J. Phys. Oceanogr*, **27**, 2087–2099. [Find this article online](#)

Drennan W. M., K. K. Kahma, and M. A. Donelan, 1999: On momentum flux and velocity spectra over waves. *Bound.-Layer Meteor*, **92**, 489–515. [Find this article online](#)

Edson J. B., S. Wetzel, C. Friehe, S. Miller, and T. Hristov, 1997: Energy flux and dissipation profiles in the marine surface layer. Preprints, *12th Symp. on Boundary Layers and Turbulence*, Vancouver, BC, Canada, Amer. Meteor. Soc., 314–315.

—, A. A. Hinton, K. E. Prada, J. E. Hare, and C. W. Fairall, 1998: Direct covariance flux estimates from mobile platforms at sea. *J. Atmos. Oceanic Technol*, **15**, 547–562. [Find this article online](#)

Elliott J. A., 1972: Microscale pressure near waves being generated by the wind. *J. Fluid Mech*, **54**, 427–448. [Find this article online](#)

Fairall C. W., and S. E. Larsen, 1986: Inertial dissipation methods and turbulent fluxes at the air–ocean interface. *Bound.-Layer Meteor*, **34**, 287–301. [Find this article online](#)

—, E. F. Bradley, D. P. Rogers, J. B. Edson, and G. S. Young, 1996a: Bulk parameterization of air–sea fluxes in TOGA COARE. *J. Geophys. Res*, **101**, 3747–3764, (C2),.

—, J. S. Godfrey, G. A. Wick, J. B. Edson, and G. S. Young, 1996b: Cool-skin and warm layer effects on sea surface temperature. *J. Geophys. Res*, **101**, 1295–1308, (C1),.

—, A. A. Grachev, A. J. Bedard, and R. T. Nishiyama, 1996c: Wind, wave, stress, and surface roughness relationships from turbulence measurements made on R/P FLIP in the SCOPE Experiment. NOAA Tech. Memo. ERL ETL-268, 37 pp. [Available from National Technical Information Service, 5285 Port Royal Rd., Springfield, VA 22161].

—, A. B. White, J. B. Edson, and J. E. Hare, 1997: Integrated shipboard measurements of the marine boundary layer. *J. Atmos. Oceanic Technol*, **14**, 338–359. [Find this article online](#)

Geernaert G. L., F. Hansen, M. Courtney, and T. Herbers, 1993: Directional attributes of the ocean surface wind stress vector. *J. Geophys. Res*, **98**, 16 571–16 582.

Godfrey J. S., and A. C. M. Beljaars, 1991: On the turbulent fluxes of buoyancy, heat, and moisture at the air–sea interface at low wind speeds. *J. Geophys. Res*, **96**, 22 043–22 048.

Grachev A. A., and C. W. Fairall, 1997: Dependence of the Monin–Obukhov stability parameter on the bulk Richardson number over the ocean. *J. Appl. Meteor*, **36**, 406–414. [Find this article online](#)

—, —, and S. S. Zilitinkevich, 1997: Surface-layer scaling for the convection-induced stress regime. *Bound.-Layer Meteor*, **83**, 423–439, (3),. [Find this article online](#)

—, —, and S. E. Larsen, 1998: On the determination of the neutral drag coefficient in the convective boundary layer. *Bound.-Layer Meteor*, **86**, 257–278, (2),. [Find this article online](#)

Hare J. E., T. Hara, J. B. Edson, and J. M. Wilczak, 1997: A similarity analysis of the structure of airflow over surface waves. *J. Phys. Oceanogr*, **27**, 1018–1037. [Find this article online](#)

Harris D. L., 1966: The wave-driven wind. *J. Atmos. Sci*, **23**, 688–693. [Find this article online](#)

Hsu C.-T., E. Y. Hsu, and R. L. Street, 1981: On the structure of turbulent flow over a progressive water wave: Theory and experiment in a transformed, wave-following coordinate system. *J. Fluid Mech*, **105**, 87–117. [Find this article online](#)

Huang N. E., L. F. Bliven, S. R. Long, and P. S. DeLeonibus, 1986: A study of the relationship among wind speed, sea state, and the drag coefficient for a developing wave field. *J. Geophys. Res*, **91**, 7733–7742.

Janssen P. A. E. M., 1989: Wave-induced stress and the drag of air flow over sea waves. *J. Phys. Oceanogr*, **19**, 745–754. [Find this article online](#)

—, 1991: Quasi-linear theory of wind wave generation applied to wave forecasting. *J. Phys. Oceanogr*, **21**, 1631–1642. [Find this article online](#)

Kinsman B., 1965: *Wind Waves, Their Generation and Propagation on the Ocean Surface*. Prentice-Hall, 676 pp.

Kitaigorodskii S. A., 1970: *The Physics of Air–Sea Interaction*, Hydrometeoizdat, Leningrad, 284 pp. (Translated from Russian by A. Baruch, Israel Program for Scientific Translations, 1973, 273 pp.).

Lai R. J., and O. H. Shemdin, 1971: Laboratory investigation of air turbulence above simple water waves. *J. Geophys. Res*, **76**, 7334–7350.

Li P. Y., 1995: A numerical study on energy transfer between turbulent air flow and finite amplitude water waves. Ph.D. thesis, York University, 181 pp.

Makin V. K., V. N. Kudryavtsev, and C. Mastenbroek, 1995: Drag of the sea surface. *Bound.-Layer Meteor*, **73**, 159–182. [Find this article online](#)

Makova V. I., 1975: Features of the dynamics of turbulence in the marine atmospheric surface layer at various stages in the development of waves. *Izv. Acad. Sci. USSR, Atmos. Oceanic Phys. (Engl. Transl.)*, **11**, 177–182. [Find this article online](#)

—, 1977: Momentum and energy exchange between wind and waves various stages in the development of waves (in Russian). *Tr. Gos. Okeanogr. Inst*, **138**, 54–63.

Miles J. W., 1957: On the generation of surface waves by shear flows. *J. Fluid Mech*, **3**, 185–204. [Find this article online](#)

Nordeng T. E., 1991: On the wave age dependent drag coefficient and roughness length at sea. *J. Geophys. Res*, **96**, 7167–7174.

Phillips O. M., 1977: *The Dynamics of the Upper Ocean*. 2d ed. Cambridge University Press, 336 pp.

Pierson W. J. Jr., and L. Moskowitz, 1964: A proposed spectral form for fully developed wind seas based on the similarity theory of S. A. Kitaigorodskii. *J. Geophys. Res*, **69**, 5181–5190.

Rieder K., J. A. Smith, and R.A. Weller, 1994: Observed directional characteristics of the wind, wind stress, and surface waves on the open ocean. *J. Geophys. Res*, **99**, 22 598–22 596.

Smedman A.-S., M. Tjernström, and U. Högström, 1994: Near-neutral marine atmospheric boundary layer with no surface shearing stress: A case study. *J. Atmos. Sci*, **51**, 3399–3411. [Find this article online](#)

—, U. Högström, H. Bergström, A. Rutgersson, K. K. Kahma, and H. Pettersson, 1999: A case study of air–sea interaction during swell conditions. *J. Geophys. Res*, **104**, 25 833–25 851, (C11),.

Sullivan P. P., J. C. McWilliams, and C.-H. Moeng, 2000: Simulation of turbulent flow over idealized water waves. *J. Fluid Mech*, **404**, 47–85. [Find this article online](#)

Takeuchi K., E. Leavitt, and S. P. Chao, 1977: Effects of water waves on the structure of turbulent shear flow. *J. Fluid Mech*, **80**, 535–559. [Find this article online](#)

Volkov Yu. A., 1968: An experimental study of the characteristics of turbulence in the marine surface layer and wind-driven waves (in Russian). Ph.D. thesis, Institute of Oceanology, Russian Academy of Science, Moscow, Russia, 132 pp.

—, 1969: The spectra of velocity and temperature fluctuations in airflow above the agitated sea-surface. *Izv. Acad. Sci. USSR, Atmos. Oceanic Phys. (Engl. Transl.)*, **5**, 723–730, (12),. [Find this article online](#)

—, 1970: Turbulent flux of momentum and heat in the atmospheric surface layer over a disturbed sea-surface. *Izv. Acad. Sci. USSR, Atmos. Oceanic Phys. (Engl. Transl.)*, **6**, 770–774, (12),. [Find this article online](#)

Wetzel S. W., 1996: An investigation of the wave-induced momentum flux through phase averaging of open ocean wind and wave fields. M.S. thesis, Joint Program in Applied Ocean Physics and Engineering, Massachusetts Institute of Technology and Woods Hole Oceanographic Institution, Woods Hole, MA, 93 pp.

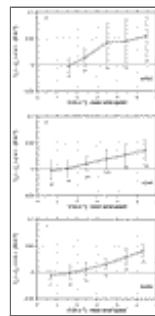
Tables

TABLE 1. The averaged uw component of the momentum flux, $\tau_x = -\rho_a \langle uw \rangle$, for light winds (up to 2 m s^{-1}) sorted according to the relative wind–swell directions based on the measurements made in ASTEX, TOGA COARE, and SCOPE

Wind speed range (m s^{-1})	Experiment	Mean momentum flux, $\tau_x = -\rho_a \langle uw \rangle$ (N m^{-2})		
		Total	Following swell	Counter-swell
0–0.9	TOGA COARE	–0.0033	–0.0054	+0.0020
	SCOPE	–0.0063	–0.0070	–0.0050
1.0–1.9	ASTEX	–0.0021	–0.0061	+0.0011
	TOGA COARE	+0.0012	+0.0006	+0.0022
	SCOPE	–0.0009	–0.0016	+0.0090

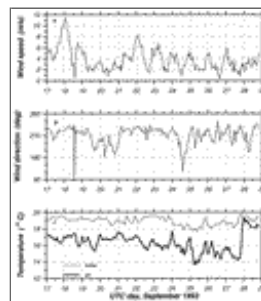
[Click on thumbnail for full-sized image.](#)

Figures



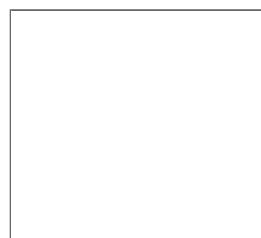
[Click on thumbnail for full-sized image.](#)

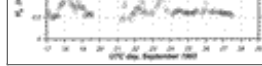
FIG. 1. The averaged uw component of the momentum flux, $\tau_x = -\rho_a \langle uw \rangle$, determined by the eddy correlation method vs mean wind speed for light and moderate wind speed ($U \leq 6 \text{ m s}^{-1}$) based on the measurements made in (a) ASTEX, (b) TOGA COARE, and (c) SCOPE. The solid lines represent the averaged momentum flux. The mean value points have been averaged in wind speed bins with 1 m s^{-1} width. Standard error bars are shown. The numbers below each bar represent the number of points averaged



[Click on thumbnail for full-sized image.](#)

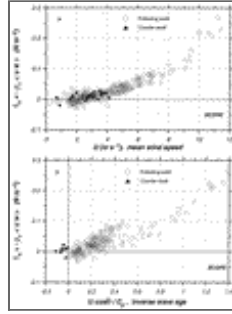
FIG. 2. Meteorological conditions during SCOPE: (a) wind speed and (b) wind direction derived from a sonic anemometer measurements, and (c) air (solid line) and water (thin line) temperature





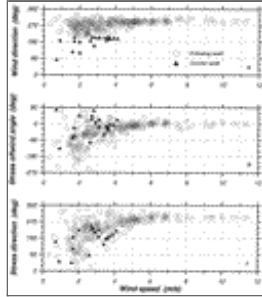
Click on thumbnail for full-sized image.

FIG. 3. Surface stress and wave conditions during SCOPE: (a) downwind, $\tau_x = -\rho_a \langle uw \rangle$ (solid line), and crosswind, $\tau_y = -\rho_a \langle vw \rangle$ (thin line), stress components, (b) wave age, and (c) significant wave height



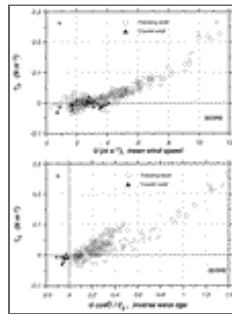
Click on thumbnail for full-sized image.

FIG. 4. Individual observations (50-min averaged) of uw component of the momentum flux (eddy correlation) vs (a) wind speed and (b) inverse wave age, $U \cos\theta/c_p$, for SCOPE data; c_p is the phase speed at the peak of the wave spectrum and θ is the relative angle between the wind and the wave direction. A positive sign of τ_x corresponds to downward momentum transfer and vice versa. Open circles represent cases when wind follows swell, and triangles are counterswell runs



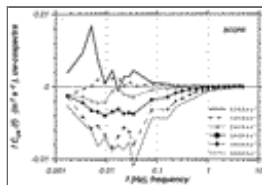
Click on thumbnail for full-sized image.

FIG. 5. Wind and stress directions as function of wind speed: (a) the true wind direction, (b) stress offwind angle, and (c) the true stress direction. All angles are calculated using the meteorological convention (“from”), e.g., 270° means wind (or stress) is from the west, and (b) negative angles correspond to counterclockwise rotation. Nomenclature is the same as in [Fig. 4](#)



Click on thumbnail for full-sized image.

FIG. 6. Surface stress component in the swell direction, τ_θ for SCOPE data vs (a) wind speed and (b) inverse wave age, $U \cos\theta/c_p$; τ_θ is derived from [Eq. \(5\)](#). Nomenclature is the same as in [Fig. 4](#)



Click on thumbnail for full-sized image.

FIG. 7. Mean cospectra $C_{uw}(f)$ of the downwind (uw) stress component [see [Eq. \(3\)](#)] for light and moderate winds based on the

SCOPE observations. The mean curves have been averaged in wind speed bins with 1 m s^{-1} width. Negative values of cospectra curves correspond to downward momentum transfer (i.e., from atmosphere to ocean)

* Additional affiliation: A. M. Obukhov Institute of Atmospheric Physics, Russian Academy of Sciences, Moscow, Russia

Corresponding author address: Dr. Andrey A. Grachev, NOAA/Environmental Technology Laboratory, R/ET7, 325 Broadway, Boulder, CO 80305-3328. E-mail: andrey.grachev@noaa.gov

top ▲



© 2008 American Meteorological Society [Privacy Policy and Disclaimer](#)
Headquarters: 45 Beacon Street Boston, MA 02108-3693
DC Office: 1120 G Street, NW, Suite 800 Washington DC, 20005-3826
amsinfo@ametsoc.org Phone: 617-227-2425 Fax: 617-742-8718
[Allen Press, Inc.](#) assists in the online publication of *AMS* journals.